



## Research Paper

## Distribution of rare earth elements and implication for Ce anomalies in the clay-sized minerals of deep-sea sediment, Western Pacific Ocean

Yan Liu<sup>a,\*</sup>, Yuntao Jing<sup>a,b</sup>, Wancang Zhao<sup>b,\*</sup><sup>a</sup> Institute of Geology, Chinese Academy of Geological Sciences, Beijing 100037, PR China  
<sup>b</sup> School of Geographical Sciences, Southwest University, Chongqing 400715, PR China

## ARTICLE INFO

**Keywords:**  
Clay-sized minerals  
Deep-sea sediments  
REY enrichment  
Iron phase  
Ce anomaly

## ABSTRACT

Recent studies reveal that bioapatite and Fe–Mn micro-nodules are predominantly hosts of rare earth elements and yttrium (REYs) in bulk deep-sea sediments by in-situ analysis and chemical extraction. However, individual clay-sized fraction (<2 μm; CSFS) could also be an important REY carriers, in which chemical species and distribution of REYs are unclear. In order to clarify the REY migration or cycle and light/heavy REE enrichment mechanism in different clay-sized minerals, this study undertook clay-sized separation, sequential chemical extraction, X-ray diffraction (XRD), X-ray fluorescence spectrometer (XRF) and inductively coupled plasma–mass spectrometry (ICP-MS) analysis of REY-rich sediment samples from two sites in the western Pacific Ocean. The results show the REY in CSFS are mainly hosted in the amorphous Fe phase ( $\text{Fe}_{\text{ox}1}$ ), with lesser amounts in carbonate and the crystalline Fe phase ( $\text{Fe}_{\text{ox}2}$ ), with average proportions of 68.0%, 27.5%, and 2.9% at site 30, and 75.2%, 16.2%, and 7.1% at site 64, respectively. The bulk sediments and CSFS show no obvious Eu anomalies, suggesting there was limited hydrothermal input. Carbonate may be an authigenic phase that inherited the REY characteristics of seawater by substituting for  $\text{Ca}^{2+}$ , and organic degradation resulted in larger negative Ce anomalies than in seawater. The ΣREY contents increase and the heavy REEs are more readily adsorbed onto the  $\text{Fe}_{\text{ox}1}$  under oxidizing conditions. The  $\text{Fe}_{\text{ox}2}$  phase may be transformed from  $\text{Fe}_{\text{ox}1}$ , which facilitates the release of light REEs. The negative Ce anomalies in Fe phase minerals are not solely caused by the depositional reduce conditions because an obvious change of Ce anomaly in different iron phase minerals.

## 1. Introduction

Deep-sea REY-rich sediments with high contents of rare earth elements and Y (REY; especially the heavy REE [Gd–Lu] and Y) are a promising mineral resource (Kato et al., 2011). In particular, in the Pacific Ocean, deep-sea sediments with ΣREY contents of several thousand parts per million (ppm) have been found and attracted wide attention (Kato et al., 2011; Iijima et al., 2016; Ohta et al., 2016; Yasukawa et al., 2018; Takaya et al., 2018; Tanaka et al., 2020; Zawadzki et al., 2020; Ren et al., 2021; Shi et al., 2021). The REY enrichment can be interpreted by two-stage fluid–bioapatite fossil interactions and minor contributions from Fe–Mn micro-nodules under an oxidized depositional environment and slow sedimentation rate (Deng et al., 2017, 2022; Zhou et al., 2021; Liao et al., 2022). The first stage is the initial adsorption of REY from seawater by shallow sediment (e.g. bioapatite and Fe–Mn mineral) at the sediment–water interface (Zhou et al., 2021). The second stage occur at deep burial sediment, REY

release into pore water with the dissolution of Fe–Mn (oxyhydr)oxides (Haley et al., 2004) and clay mineral (Abbott et al., 2019). Then bioapatite can absorb REY from pore water during diagenetic process. During these processes, the Fe–Mn micro-nodules are the REY carriers and the bioapatite is the main REY host, as inferred from in situ analyses (Bi et al., 2021; Zhou et al., 2021; Kon et al., 2014; Liao et al., 2019a) and simple chemical extraction approaches (Takaya et al., 2015; Ren et al., 2022). Various Fe–Mn (oxyhydr)oxide phases (i.e., hydrogenetic, hydrothermal, and diagenetic), particularly micro-nodules, are additional significant REY hosts (Yasukawa et al., 2014a, 2014b, 2020; Liao et al., 2019b; Zhou et al., 2020). In addition, phillipsite that forms at low sedimentation rates (Kato et al., 2011; Yasukawa et al., 2014a, 2014b; Ohta et al., 2016) and clay minerals (Abbott et al., 2019) have the potential to host REY in deep-sea sediments.

A key issue regarding REY-rich sediments is to constrain the actual proportions of REY held by each mineral phase in the sediment. Sequential extraction is commonly used for quantitatively

\* Corresponding authors.

E-mail addresses: [ly@cags.ac.cn](mailto:ly@cags.ac.cn) (Y. Liu), [zhwc321@163.com](mailto:zhwc321@163.com) (W. Zhao).

characterizing and chemically isolating individual mineral phases (Poulton and Canfield, 2005). In recent studies, sequential leaching experiments on bulk sediment samples from the Pacific Ocean have shown the REY are primarily hosted in phosphates (~70%) and Fe–Mn (oxyhydr)oxides (including Fe–Mn micro-nodules and fine-grained Fe–Mn minerals), and that hydrothermal Fe (oxyhydr)oxides can accumulate more REY than Mn(oxyhydr)oxides (Kim et al., 2022; Liao et al., 2022). Clay mineral may be an important REY host phase, and its dissolution and authigenesis are likely greatly influences the marine REY cycling (Abbott et al., 2019). The REY contents are also controlled by the grain size, and smaller grain size have higher P, Mn and REY content (Sa et al., 2018). However, few studies have quantified the REY hosts in clay-sized sediments (<2 µm), which contain abundant fine-grained Fe–Mn (oxyhydr)oxides and clay minerals and could scavenge much REY from seawater. Interface reactions usually occur between Fe–Mn-bearing minerals and seawater, including surface adsorption, redox reaction and surface ectopic catalytic reaction (Hochella Jr., 1990; Stumm, 1992; Halbach and Puteanus, 1984; Takahashi et al., 2007; Ohta and Kawabe, 2000; Hein and Koschinsky, 2014), resulting these phases transformation and accumulate a large amount of REY. Some experiments have shown that the light REEs are preferentially absorbed onto synthetic Fe and Mn (oxyhydr)oxides as compared with the heavy REEs (Koeppenkastrop and De Carlo, 1992; Ohta and Kawabe, 2000). Jiang et al. (2011) proposed that amorphous Fe (oxyhydr)oxides in hydrogenic Fe–Mn crusts incorporate mainly free REY<sup>3+</sup>, whereas δMnO<sub>2</sub> incorporates REY–carbonate complexes from seawater.

In this study, we quantified the proportion and fraction of  $\sum$ REY in each clay-sized phases after clay separation and sequential chemical extraction, based on the method of Lu et al. (2017), and X-ray diffraction (XRD), X-ray fluorescence spectrometer (XRF) and inductively coupled plasma–mass spectrometry (ICP–MS) techniques. Our key objective is to clarify marine REY migration or cycle and light/heavy REE enrichment mechanism in different clay-sized minerals.

## 2. Materials and methods

We analyzed 18 and 9 REY-rich deep-sea sediment samples from sites 64 and 30, respectively. These REY-rich sediment samples were obtained by the R/V *Haiyangdizhi-6* in the Pigafetta Basin in the western Pacific Ocean in 2014 from a water depth of ~6000 m (Fig. 1). We use the equipment of piston corer to collect the sediment samples. But deep sea sediment at site 30 were collected from 15 to 300 cm below the seafloor (cmbsf) and samples at site 64 were collected from 15 to 630 cmbsf. The samples were collected 15 cm depth intervals to identify the changes in clay-sized mineralogy and REY contents with depth. These REY-rich sediment samples are generally brown to black. Such samples have even and loose texture and individual mineral grains are nearly invisible on hand specimen. Sequential chemical extraction was undertaken on 27 samples with various Fe and REY contents (Table S1).

### 2.1. Separation of the clay-sized fraction

The clay-sized fraction was separated from bulk sediment samples based on a procedure optimized from Ji et al. (1999). The clay-sized fraction was separated by centrifuging for 3 min at 2000 r/min. The clay-sized fraction was then collected from the suspended solution by centrifuging for 15 min at 5000 r/min.

### 2.2. X-ray diffraction analysis

In this study, clay-sized fractions separated from bulk sediment samples were used to make oriented sections. Then, each oriented sections were analyzed by a Rigaku D/Max-rB diffractometer with Cu-Kα radiation under dry air conditions and glycolated treated at a voltage of 35 kV and a current of 15 mA, respectively. These oriented sections were scanned with a goniometer from 3° to 36° 2θ stepped by 0.01° (Moore and Reynolds, 1997). The detailed procedure was described by Lu et al. (2017) and Zhao et al. (2018). Based on the positions of the (001) series

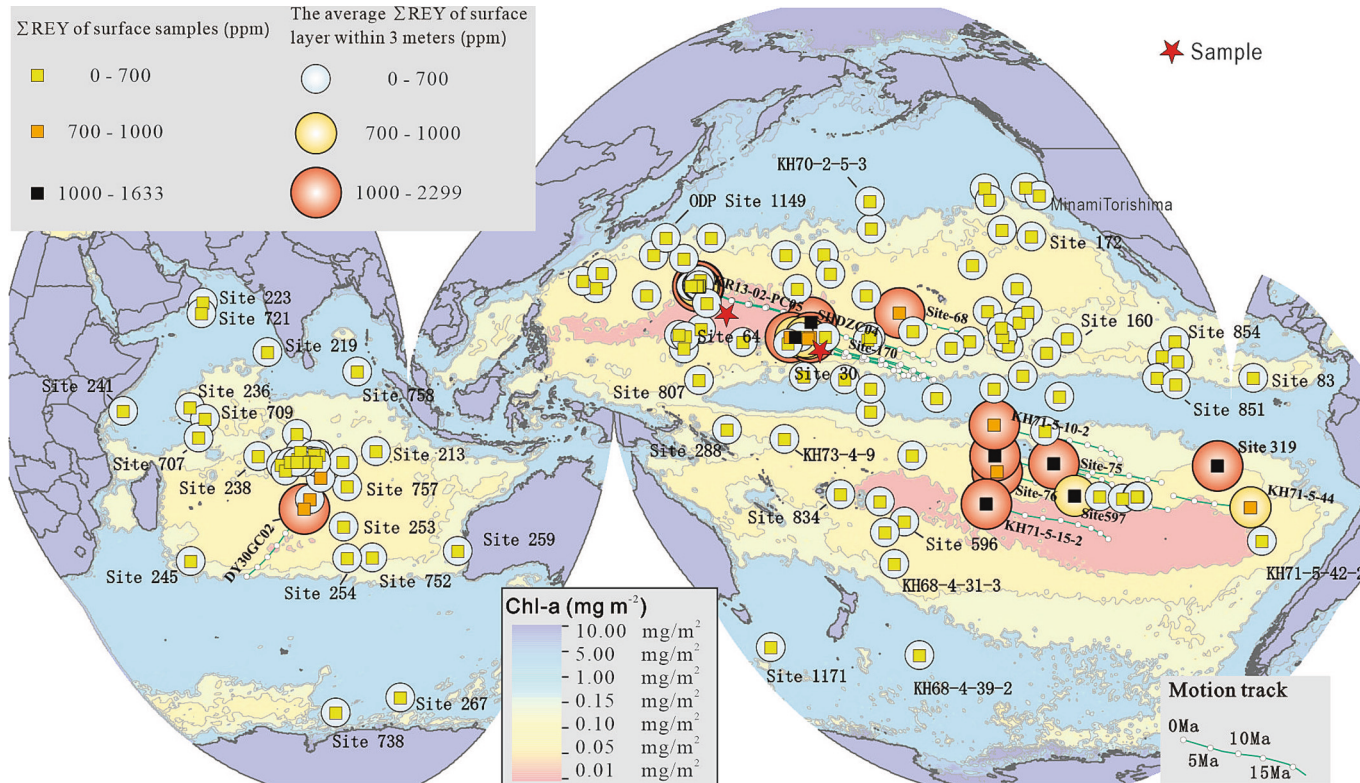


**Fig. 1.** Locations of sampling sites of deep-sea sediments from the Pacific and Indian oceans (modified from Ren et al., 2021).

of basal reflections on the XRD powder diagrams, main clay minerals compositions (i.e., smectite, illite and kaolinite + chlorite) can be identified based on the air-dried and glycolated curve made by the XRD diagram (Fig. S1, Table S5). Semi-quantitative calculations of smectite (17 Å), illite (10 Å) and kaolinite + chlorite (7 Å) were performed by MDI JADE 6 software with peak height, and the corresponding intensification factors are 1, 4 and 2, respectively (Cook et al., 1975). The deviation of this method is estimated to be about 8–10% of the relative abundance of individual clay minerals.

### 2.3. Sequential chemical extraction

The sequential chemical extraction procedure is followed the method of Lu et al. (2017), which in turn was modified from Poulton and Canfield (2005). In this study, approximate 100 mg of CSFS samples were weighed and performed 5 steps to extract REYs from different mineral phases.

Step 1: 5 mL of 1 M acetic acid was applied to dissolve carbonate. It is noted that 1 M Na acetate can be used in sequential leaching experiments to extract carbonate and authigenic or biogenic phosphates together (Ruttenberg, 1992; Kim et al., 2022; Liao et al., 2022). Given the large grain size of bioapatite (50–500 µm; Ohta et al., 2016; Sa et al., 2018; Bi et al., 2021; Zhou et al., 2021; Ren et al., 2022), the acetic acid used in this study mainly removes carbonates rather than phosphates.

Step 2: After step 1, the precipitate reacted with a mixture of 37.5 mL of 1 M hydroxylamine hydrochloride and 12.5 mL acetic acid to dissolve amorphous iron phase (easily reducible Fe oxides;  $\text{Fe}_{\text{ox}1}$ ; e.g., ferrihydrite and lepidocrocite, Poulton and Canfield, 2005). After mixing completely, the samples were placed under dark conditions for 24 h.

Step 3: Following by step 2, a mixture of CBD (45 mL of 0.3 M citrate, 5 mL of 1 M bicarbonate solution and excess dithionite powder) were used to dissolve crystalline iron phase (reducible Fe oxides;  $\text{Fe}_{\text{ox}2}$ ; for example hematite and goethite; Mehra and Jackson, 1958). After shaking for 30 min at 90 °C, the color of the residues changes from brown to green-gray.

Step 4: After step 3, 3 mL boiling of 6 M HCl was selected to extract REYs from phyllosilicate minerals ( $\text{Fe}_{\text{HCl}}$ ; e.g., smectite and chlorite; Poulton and Canfield, 2005). After boiling for 2 h, the color of the residues changes from green-gray to white. Then the volume was adjusted to 15 mL with pure water.

Step 5: After step 4, a mixture of *aqua regia* and HF solution was applied to dissolve residual Fe phase ( $\text{Fe}_R$ ; e.g., illite). The residual samples added with 4 mL *aqua regia* were heated at 130 °C for 2 h until evaporated to dryness. Then, the residual phase was dissolved with 1 mL HF until it was completely dissolved. Eventually, the volume was adjusted to 15 mL by addition of 0.1 M  $\text{HNO}_3$ .

After the reaction of every extraction step, the samples and reagent were centrifuged for 15 min at 5000 r/min and the contents of REY were measured in the diluted supernatant liquids by ICP-MS (Tables S4–S5). The element contents in each dissolved phases respect to clay-sized sediment composition were calculated by the contents in each extracted solution multiply by the volume of added solution and divided by initial mass of clay-sized sediment.

It was assumed that crystalline Fe was formed by transformation of amorphous Fe. This process may be accompanied by hydrolysis of  $\text{Fe}^{3+}(\text{aq})$ , oxidation of  $\text{Fe}^{2+}(\text{aq})$ , and Fe(II) catalysis (Sheng et al., 2020; Li et al., 2022). As such, the  $\text{Fe}_{\text{Feox1}}/\text{Fe}_{\text{Feox2}}$  ratio might be a proxy for reducing processes.

### 2.4. Chemical analysis

Major elements analyses were performed at ALS Chemex (Guangzhou) Co Ltd. This analyses were conducted on XRF (PANalytica, PW2424, Netherlands); analytical errors were estimated to be <5% relative. Sample powder was mixed with lithium borate - lithium nitrate melting flux. After fully mixing, it was placed in the furnace to melt at

high temperature. Then, this melting sample was quenched with air for 1 min to produce flat discs on the fire birck for the XRF analyses.

Sample digestion was undertaken at Guizhou Tongwei Analytical Technology Co., Ltd. The trace element were measured by Thermo Fisher ICP-MS X2. The ICP-MS procedure for trace element analysis follows the protocol by Egginis and modified by the Radiogenic Isotope Laboratory (Egginis et al., 1997; Kamber et al., 2003; Lawrence et al., 2006). Samples were analyzed on a Thermal X series 2 equipped with an ESI SC-4 DX FAST autosampler. A screen was used and the operating conditions were optimized for highest sensitivity with low oxides rate (<2%  $\text{CeO}/\text{Ce}$ ). 4 repeats of 131 sweeps at one point with dwell times of 5–15 ms for each analytes. Isobar and polyatomic interferences were corrected using the formation rates measured with pure single element REY and Ba after each experiment. Apart from  $\text{BaO}+$  interference on Eu, all other oxide interference, especially on REY have been corrected. USGS W2a was used as reference standard and crossed checked with BIR-1, BHVO-2 and JCp-1. Instrument drift mass bias were corrected with internal standards and external monitors. The results and relative standard deviations are in ppb and 1 sigma. The  $\delta\text{Ce}$  and  $\delta\text{Eu}$  values were calculated as follows:  $\delta\text{Ce} = 2\text{Ce}_N/(\text{La}_N + \text{Pr}_N)$  and  $\delta\text{Eu} = 2\text{Eu}_N/(\text{Sm}_N + \text{Gd}_N)$ , where N denotes normalization to the North American Shale Composite (NASC; Gromet et al., 1984).

## 3. Results

### 3.1. Chemical compositions of bulk REY-rich sediment and their clay-sized fraction

The chemical compositions of the REY-rich bulk sediments and clay-sized fractions from site 30 and 64 are presented in Table S1–S3. The bulk sediments from site 30 show the contents of  $\text{Fe}_2\text{O}_3$ ,  $\text{MnO}$ ,  $\text{CaO}$ ,  $\text{P}_2\text{O}_5$  are 6.11–7.64%, 1.18–1.52%, 1.85–2.65%, 0.85–1.37%, respectively and moderate  $\sum\text{REY}$  contents of 498–865 ppm (Table S1). The NASC-normalized REY patterns exhibit heavy REEs enrichment, no obvious Eu anomalies (average = 1.02) and obvious negative Ce anomalies (average = 0.39). The site 64 bulk sediments show the contents of  $\text{Fe}_2\text{O}_3$ ,  $\text{MnO}$ ,  $\text{CaO}$ ,  $\text{P}_2\text{O}_5$  are 6.17–9.54%, 1.91–3.61%, 2.64–5.52%, 1.32–3.53%, respectively and high  $\sum\text{REY}$  contents of 782–1971 ppm (Table S1). The NASC-normalized REY patterns exhibit heavy REEs enrichment, no obvious Eu anomalies (average = 0.97) and obvious negative Ce anomalies (average = 0.41) (Fig. 2A–B).

The clay-sized fractions from site 30 show the  $\text{Fe}_2\text{O}_3$ ,  $\text{MnO}$ ,  $\text{CaO}$ ,  $\text{P}_2\text{O}_5$  contents are 9.48–10.86%, 1.58–2.24%, 1.74–2.96%, 0.73–1.78% (Table S2), with higher Fe and Mn content than bulk sediment and  $\sum\text{REY}$  contents are 321–1032 ppm (Table S3). The NASC-normalized REY patterns exhibit heavy REEs enrichment, no obvious Eu anomalies (average = 1.08) and obvious negative Ce anomalies (average = 0.53) (Fig. 2C–D). The clay-sized fractions from site 64 show the  $\text{Fe}_2\text{O}_3$ ,  $\text{MnO}$ ,  $\text{CaO}$ ,  $\text{P}_2\text{O}_5$  contents are 9.06–13.72%, 3.63–5.43%, 2.48–4.16%, 1.24–2.54% (Table S2), with higher Fe and Mn content than bulk sediment and high  $\sum\text{REY}$  contents of 997–3505 ppm (Table S3). The NASC-normalized REY patterns exhibit heavy REEs enrichment, no obvious Eu anomalies (average = 1.08) and obvious negative Ce anomalies (average = 0.50) (Fig. 2C–D).

### 3.2. Mineral composition of CSFS

Clay-sized minerals XRD analyses (Fig. S1 Table S6) show the mainly minerals are smectite, followed by illite, kaolinite and a few samples may contain chlorite. The diffraction peaks of Fe and Mn phase minerals and hydroxyapatite could not be recognized. It is probably that the characteristic peaks of Fe—Mn (hydroxide) oxide (e.g. vernadite, birnessite, todorokite, lepidocrocite, goethite, hematite) are covered by clay mineral or the crystallinity of these phases was very low or these minerals occurred in disperse phases (Shi et al., 1995). The hydroxyapatite is rare in clay-sized fraction.

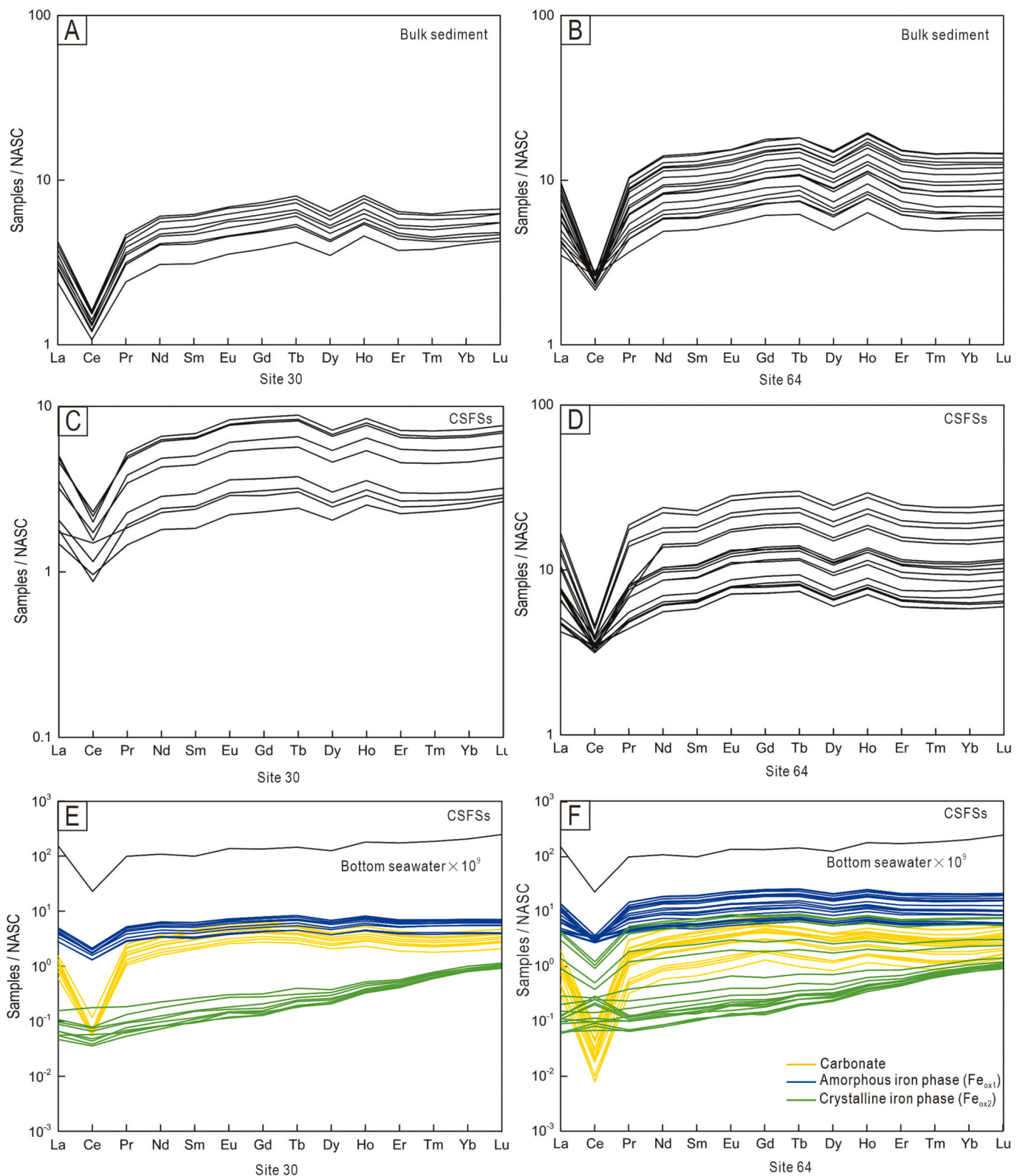


**Fig. 2.** NASC-normalized REY patterns for (A–B) bulk sediments at sites 30 and 64, respectively, (C–D) clay-sized fraction at sites 30 and 64, respectively, and the (E–F) carbonate, and amorphous iron phase ( $Fe_{ox1}$ ) and crystalline iron ( $Fe_{ox2}$ ) phase in the clay-sized fraction of deep-sea sediment. NASC normalizing values are from Gromet et al. (1984). Data for seawater are from Deng et al. (2017), which was collected at a water depth of 5663 m in the western Pacific.

### 3.3. Sequential chemical extraction

The REY elements concentration of the solution in the sequential chemical extraction experiment are summarized in Table 1, and the

detailed data are listed in Table S4-S5.

Carbonate extracted in step 1 has Ca, Mg, Fe, Mn contents of 6724–10,172 ppm, 2652–3927 ppm, 644–1509 ppm, 251–438 ppm at site 30 and 8174–13,982 ppm, 2114–3668 ppm, 183–1812 ppm,

**Table 1**

Summary of characteristics of REY in carbonate,  $\text{Fe}_{\text{ox}1}$ ,  $\text{Fe}_{\text{ox}2}$ ,  $\text{Fe}_{\text{HCl}}$ , and  $\text{Fe}_{\text{R}}$  in the clay-sized fraction of deep-sea sediments after five sequential chemical extraction steps.

Treatment	sites	$\delta\text{Eu}$	$\delta\text{Ce}$	LREE/HREE	$\Sigma\text{REY}$ (ppm)
Step 1 Carbonate phase	site 30	1.06–1.09	0.04–0.07	0.73–0.88	200–464
	site 64	0.92–1.08	0.02–0.05	0.54–0.87	94.5–564
Step 2 Amorphous Fe–Mn phase ( $\text{Fe}_{\text{ox}1}$ )	site 30	1.02–1.05	0.40–0.47	1.19–1.36	557–1001
	site 64	1.02–1.07	0.24–0.77	1.01–1.57	837–2740
Step 3 Crystalline iron phase ( $\text{Fe}_{\text{ox}2}$ )	site 30	1.00–1.24	0.61–1.04	0.39–0.93	25.1–54.7
	site 64	0.96–1.18	0.24–2.30	0.50–1.21	29.2–912
Step 4 Phyllosilicate minerals ( $\text{Fe}_{\text{HCl}}$ )	site 30	1.19–2.34	0.76–0.92	4.64–6.67	6.87–23.3
	site 64	0.86–2.34	0.36–1.01	1.68–9.33	13.9–114
Step 5 Residual phase ( $\text{Fe}_{\text{R}}$ )	site 30	–	0.80–0.95	4.17–7.50	1.05–7.79
	site 64	2.34	0.53–1.11	1.89–6.60	3.13–8.17

218–913 ppm at site 64, respectively (Table S4). The relatively low Mg, Fe, and Mn contents (<4000 ppm) suggests Ca carbonate is the main mineral. The  $\Sigma\text{REY}$  contents and the light/heavy REE ratios are

200–464 ppm, 0.73–0.88 at site 30 and 94.5–564 ppm, 0.54–0.87 at site 64, respectively (Table 1). The Ca contents exhibit a negative correlation with light/heavy REE ratios at both sites (Fig. 3A). The NASC-normalized REY patterns exhibit heavy REEs enrichment, no obvious Eu anomalies (average = 1.07 at site 30, 1.01 at site 64) and obvious negative Ce anomalies (average = 0.05 at site 30, 0.03 at site 64) (Fig. 2E–F).

Amorphous Fe–Mn extracted in step 2 from the site 30 samples has Fe contents of 3888–5888 ppm, Mn contents of 9960–16,535 ppm, and Mn/Fe ratios of 1.75–3.73, which are lower than the Fe contents of 7700–16,254 ppm, Mn contents of 25,395–42,800 ppm, and Mn/Fe ratios of 2.02–5.04 at site 64 (Table S4). Given that Mn and Fe occur in different phases rather than a single phase (Liao et al., 2019b, 2022; Kim et al., 2022), there are more Mn minerals (e.g., vernadite, birnessite, and todorokite) than amorphous Fe (oxyhydr)oxide minerals (e.g., ferrihydrite and lepidocrocite). The  $\Sigma\text{REY}$  contents vary from 557 to 1001 ppm at site 30 and 837 to 2740 ppm at site 64, which are much higher than those for step 3. The light/heavy REE ratios are 1.19–1.36 at site 30 and 1.01–1.57 at site 64 (Table 1). The  $\Sigma\text{REY}$  contents exhibit a negative correlation with Mn and no or a negative correlation with  $\text{Fe}_{\text{Feox1}}/\text{Fe}_{\text{Feox2}}$  ratios (Fig. 3B and C), and the Fe + Mn contents exhibit a weak positive correlation with light/heavy REE ratios (Fig. 3D) at sites 30 and 64. The light/heavy REE ratios exhibit a positive correlation with  $\text{Fe}_{\text{Feox1}}/\text{Fe}_{\text{Feox2}}$  ratios at sites 30 and 64 (Fig. 3E). The NASC-normalized REY patterns exhibit heavy REEs flat, no obvious Eu anomalies (average = 1.03 at site 30, 1.04 at site 64) and obvious negative Ce anomalies (average = 0.43 at site 30, 0.44 at site 64) (Fig. 2E–F). The  $\delta\text{Ce}$  values of

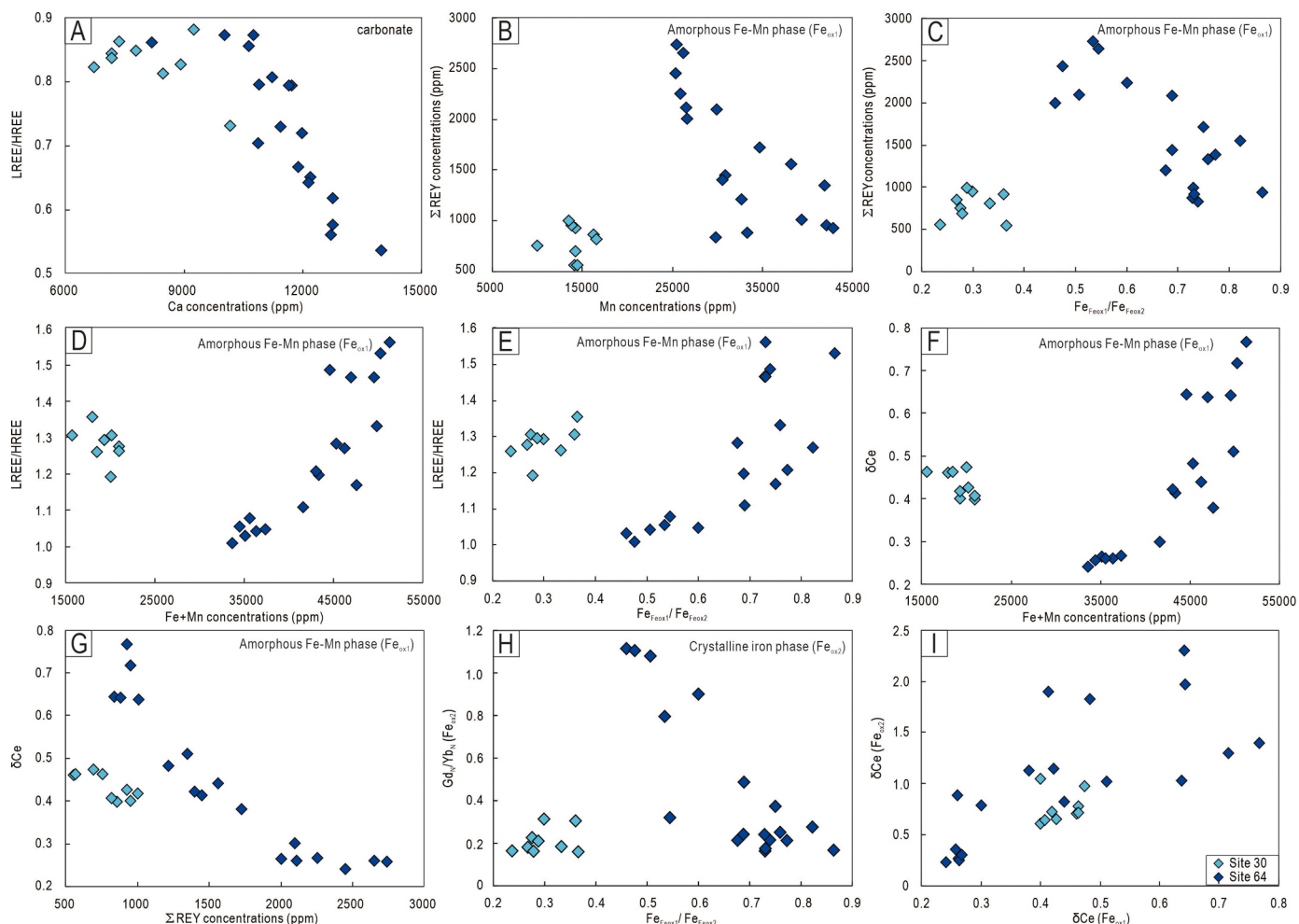


Fig. 3. Scatter plots of the chemical compositions of carbonate,  $\text{Fe}_{\text{ox}1}$ , and  $\text{Fe}_{\text{ox}2}$  in deep-sea sediment samples from the western Pacific Ocean.

$\text{Fe}_{\text{ox}1}$  exhibit a weak or positive correlation with  $\text{Mn} + \text{Fe}$  at sites 30 and 64, respectively (Fig. 3F), and the  $\Sigma\text{REY}$  contents increase gradually as  $\delta\text{Ce}$  decreases (Fig. 3G).

Crystalline Fe extracted by step 3 has  $\text{Fe} = 10,635\text{--}20,598$  ppm at site 30 and  $\text{Fe} = 9484\text{--}22,299$  ppm at site 64. The low Mn contents ( $<450$  ppm) suggest that a crystalline Fe phase is the main mineral. The

$\text{Fe}_{\text{Feox}2}/\text{Fe}_{\text{Feox}1}$  ratios are 2.74–4.23 at site 30 and 1.16–2.18 at site 64. The  $\Sigma\text{REY}$  contents vary from 25.1 to 54.7 ppm at site 30 and 29.2 to 912 ppm at site 64, and are much lower than those in  $\text{Fe}_{\text{ox}1}$ . The light/heavy REE ratios in  $\text{Fe}_{\text{ox}2}$  are 0.39–0.93 at site 30 and 0.50–1.21 at site 64. The NASC-normalized REY patterns exhibit an upward trend in heavy REEs, no obvious Eu anomalies (average = 1.07 at site 30, 1.09 at

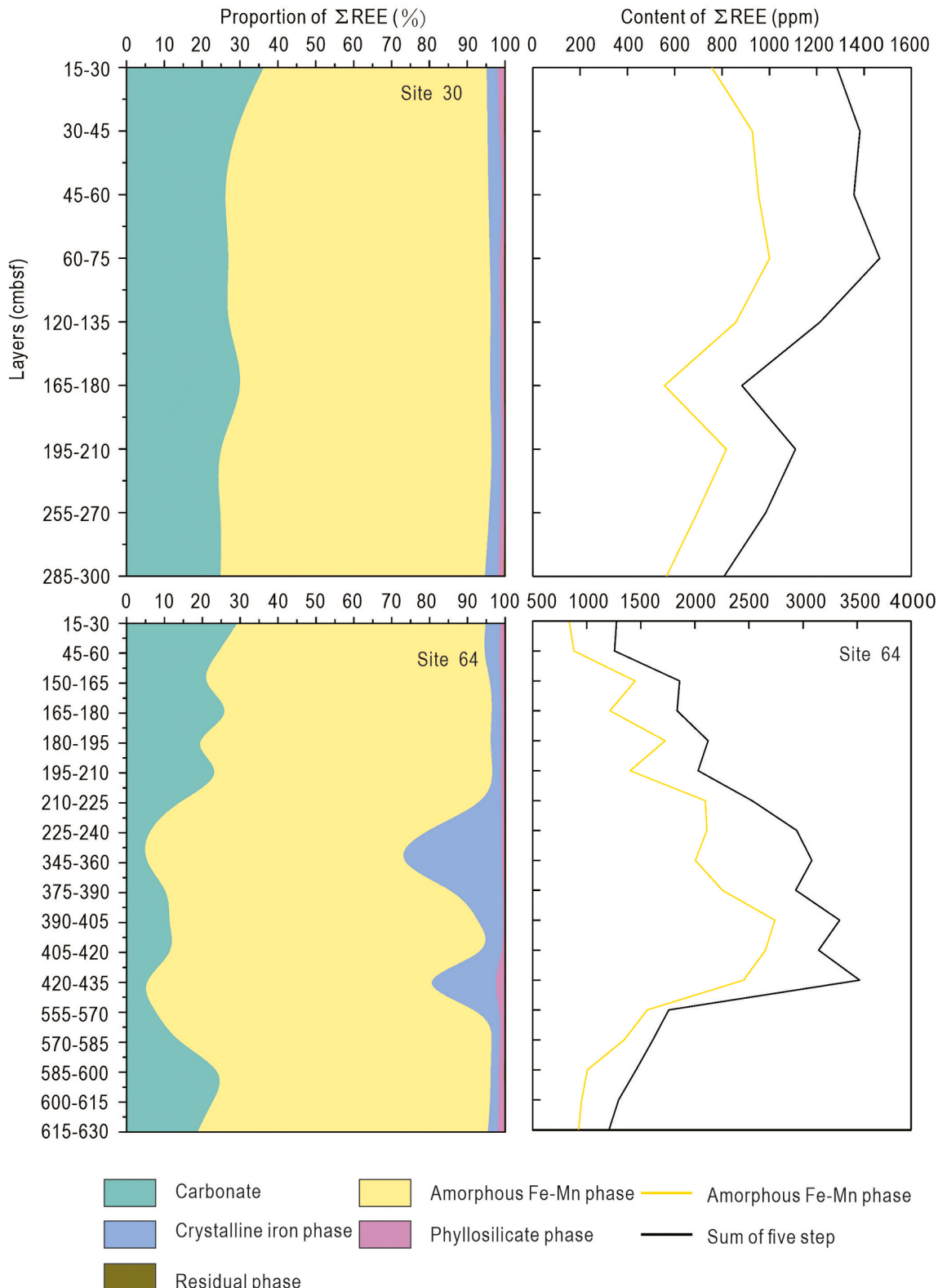


Fig. 4. Variations in REY speciation with depth in the western Pacific Ocean.

site 64) and obvious negative or positive Ce anomalies (average = 0.76 at site 30, 1.05 at site 64) (Fig. 2E–F). The HREE enrichment can be quantified by the  $Gd_N/Yb_N$  ratio, which exhibits no or a negative correlation with  $Fe_{Feox1}/Fe_{Feox2}$  ratios at sites 30 and 64 (Fig. 3H), respectively. The  $\delta Ce$  values of  $Fe_{ox2}$  exhibit a positive correlation with the  $\delta Ce$  values of  $Fe_{ox1}$  (Fig. 3I).

The main phyllosilicate mineral ( $Fe_{HCl}$ ) digested in step 4 is smectite (Fig. S1; Table S6). It has low  $\Sigma REY$  contents of 6.87–23.3 ppm at site 30 and 13.9–114 ppm at site 64. The light/heavy REE ratios are 4.64–6.67 at site 30 and 1.68–9.33 at site 64 (Table 1).

Residual iron ( $Fe_R$ ) extracted in step 5 is dominantly illite and has  $\Sigma REY$  contents of 1.05–7.79 ppm at site 30 and 3.13–8.17 ppm at site 64. The light/heavy REE ratios are 4.17–7.50 at site 30 and 1.89–6.60 at site 64, indicative of light REEs enrichment (Table 1).

The variation tendency of five REY chemical species with depth in Fig. 4. The amorphous Fe phase is main host of REY. The variation trend of  $\Sigma REY$  contents in amorphous Fe phase is consistent with those in the sum of five-step with depth at site 30 and 64. The proportion of  $\Sigma REY$  in different species show no obvious variation tendency with depth at site 30. The  $\Sigma REY$  contents in amorphous Fe phase and sum of five-step are the highest at depth of 200–500 cmbsf at site 64. The corresponding proportion of  $\Sigma REY$  in amorphous iron phase and crystalline iron phase is highest, while those in carbonate phase is lowest.

#### 4. Discussion

##### 4.1. REY hosts in the clay-sized fraction: predominantly by $Fe_{ox1}$ and subordinated by carbonate and $Fe_{ox2}$

Although the sediment samples from sites 30 and 64 exhibit REY variations, the REY patterns are similar for each step of the extraction experiments, suggesting that the REY fractionation in the clay-sized sediment is controlled mainly by the constituent minerals or oxides rather than the depositional environment (Fig. 2E–F). The Fe and Mn contents in clay-sized fraction are higher than those in bulk sediment and low P content in clay-sized fraction at site 30 and site 64 (Table S2), suggesting there are many Fe/Mn-bearing minerals and apatite is rare. Meanwhile, it also probably exists minor nano-minerals bearing P, which may influence REY species. The  $\Sigma REY$  contents of carbonate and the four Fe species in the clay-sized fraction are summarized in Table 1, and all the data for each sample are listed in Tables S4–S5.

###### 4.1.1. Carbonate

The  $\Sigma REY$  contents are 200–464 ppm at site 30 and 94.5–564 ppm at site 64 (Table 1). The light/heavy REE ratios are 0.73–0.88 at site 30 and 0.54–0.87 at site 64. The Ca contents exhibit a negative correlation with light/heavy REE ratios at both sites (Fig. 3A), suggesting that the Ca carbonate contains a higher content of heavy than light REEs. The NASC-normalized REE patterns of the Ca carbonate are similar to those of seawater. As such, the Ca carbonate may be an authigenic carbonate from seawater and inherited the REY characteristics of seawater (e.g., heavy REEs-rich with a distinct negative Ce anomaly; Deng et al., 2017; Fig. 2E–F). This involves the substitution of  $Ca^{2+}$  by  $REY^{3+}$  and maintaining charge balance by the coupled incorporation of  $Na^+$  (Voigt et al., 2017).

###### 4.1.2. Amorphous Fe–Mn phase ( $Fe_{ox1}$ )

The  $\Sigma REY$  contents vary from 557 to 1001 ppm at site 30 and 837 to 2740 ppm at site 64 for step 2, which are much higher than those for step 3. Previous studies have proposed that amorphous Fe (oxyhydr)oxides incorporate more REY than amorphous Mn minerals (Jiang et al., 2011). In this study,  $\Sigma REY$  contents exhibit a negative correlation with Mn (Fig. 3B), suggesting the REY are mainly hosted in amorphous Fe rather than Mn minerals. Given that the ionic radii of  $Fe^{3+}$  and  $Mn^{4+}$  are different from those of the  $REY^{3+}$ , isomorphous substitution is unlikely to occur. Therefore, surface adsorption, complexation, and redox

reactions may be the main mechanisms by which Fe minerals adsorb the REY from seawater (Hochella Jr., 1990; Stumm, 1992; Guan et al., 2017). The adsorption/complexation capacity of REYs onto Fe minerals is affected by the style and ability of combination (e.g. –OH) (Schindler and Stumm, 1987; Tang and Johannesson, 2005). Amorphous Fe (oxyhydr)oxides have a strong adsorption capacity due to their large specific surface area (Dzombak and Morel, 1990) and point of zero charge (PZC; ferrihydrite = 8.7; Kosmulski, 2011; lepidocrocite = 7.4; Borer et al., 2009). As such, at the pH of seawater (7.9–8.4) (Koschinsky and Hein, 2003), negatively charged species ( $HREE(CO_3)^{2-}$ ) tend to bind to slightly positively charged  $FeOOH$  phases through electrostatic adsorption (Koschinsky and Halbach, 1995; Koschinsky and Hein, 2003). More important, the amorphous Fe (oxyhydr)oxides prefer to directly combine with free  $REY^{3+}$  ions in seawater via hydroxyl ions (–OH) or oxygen bridges (Tamura et al., 2001; Jiang et al., 2011). The –OH group of Fe phases supplies adsorption sites for dissolved  $REY^{3+}$  cations or complexed ions in seawater and released  $H^+$  or hydrated ions (Tamura et al., 2001), which were connected by coordination bonds or stable inner-sphere complexes (Guan et al., 2017). The  $\Sigma REY$  contents exhibit a negative correlation with  $Fe_{Feox1}/Fe_{Feox2}$  ratios (Fig. 3C) at sites 64, suggesting that the  $\Sigma REY$  contents increase under more oxidizing conditions. The light/heavy REE ratios are 1.19–1.36 at site 30 and 1.01–1.57 at site 64 (Table 1). The Fe + Mn contents exhibit a positive correlation with light/heavy REE ratios at sites 64 (Fig. 3D), suggesting the amorphous Fe–Mn minerals preferentially incorporate light rather than heavy REEs. The light/heavy REE ratios exhibit a positive correlation with  $Fe_{Feox1}/Fe_{Feox2}$  ratios at sites 30 and 64 (Fig. 3E), suggesting the light REEs are more readily adsorbed onto  $Fe_{ox1}$  under reducing conditions via the following reaction (Tamura et al., 2001; Jiang, 2010; Guan et al., 2017):



In addition, because the Fe, Mn,  $\Sigma REY$  content in  $Fe_{ox1}$  and  $Fe_{ox2}$  at site 30 are much lower than site 64 (Table S4), suggesting the amorphous Fe are lower and stronger oxidability at site 30 than site 64. The Al and Si content in clay-sized fraction at site 30 are higher than site 64 (Table S2), implying more clay mineral at site 30 than site 64. Thus, the REY distribution and content at site 30 are controlled by low amorphous iron content, high clay mineral content (low  $\Sigma REY$  content), and strong oxidability. Thus, the  $\Sigma REY$  contents exhibit a weak correlation with  $Fe_{Feox1}/Fe_{Feox2}$  ratios (Fig. 3C) and the Fe + Mn contents exhibit a weak negative correlation with light/heavy REE ratios at sites 30 (Fig. 3D).

###### 4.1.3. Crystalline iron phase ( $Fe_{ox2}$ )

The  $\Sigma REY$  contents vary from 25.1 to 54.7 ppm at site 30 and 29.2 to 912 ppm at site 64, and are much lower than those in  $Fe_{ox1}$ . The light/heavy REE ratios in  $Fe_{ox2}$  are 0.39–0.93 at site 30 and 0.50–1.21 at site 64, indicating heavy REEs enrichment, although a few samples at site 64 exhibit light REEs enrichment (Table 1). The  $Fe_{Feox2}/Fe_{Feox1}$  ratios are 2.74–4.23 at site 30 and 1.16–2.18 at site 64, suggesting a large amount of amorphous Fe ( $Fe_{ox1}$ ) was transformed into crystalline Fe ( $Fe_{ox2}$ ). This process involves a change in structure and a decrease in the specific surface area (Stumm and Sulzberger, 1992; Raiswell and Canfield, 2012). We speculate that the light REEs are more readily excluded from  $Fe_{ox2}$  during the transformation from  $Fe_{ox1}$  to  $Fe_{ox2}$ , which corresponds to an oxidation process. The  $Gd_N/Yb_N$  ratio exhibits no or a negative correlation with  $Fe_{Feox1}/Fe_{Feox2}$  ratios at sites 30 and 64 (Fig. 3H), respectively, indicating that the heavy REEs are more readily retained on  $Fe_{ox2}$  under oxidizing conditions.

Our combined data show that carbonate,  $Fe_{ox1}$ ,  $Fe_{ox2}$ ,  $Fe_{HCl}$ , and  $Fe_R$  host an average of 27.5%, 68.0%, 2.94%, 1.14%, and 0.37% of the  $\Sigma REYs$  relative to 5-step total REY at site 30; and 16.2%, 75.2%, 7.11%, 1.20%, and 0.27% of those at site 64, respectively. As expected, the  $\Sigma REY$  contents of the first three steps account for >95% of the total REY

from the sequential chemical extraction steps, indicating that the REY in clay-sized marine sediment are bound to carbonate, amorphous Fe—Mn, and crystalline Fe phases. However, the Fe-rich smectite formed by a reaction between Fe-(oxyhydr)oxides and biogenic silica (Dymond and Eklund, 1978; Rong et al., 2018; Kim et al., 2022). It is generally considered that this process releases REY to pore waters, as the smectite structure cannot accommodate the REY (Kim et al., 2022).

#### 4.2. Does the cerium anomaly reflect the redox conditions of the depositional environment?

Redox conditions in sediments are controlled by the input of organic matter, oxygen flux, and sedimentation rate (Anderson and Sarmiento, 1995). The Ce anomaly in sediments has been widely used to assess the redox conditions of sediment deposition in marine environments (Albo and Nozaki, 1999; Pattan et al., 2005; Cao et al., 2022). However, Fe cycling, ocean circulation, terrigenous material, and hydrothermal input may complicate interpretations of the Ce anomaly (Bau, 1999; Hathorne et al., 2015; Cao et al., 2022; Zhang and Shields, 2022). Eu<sup>3+</sup> can be reduced to Eu<sup>2+</sup> during hydrothermal processes (i.e., in a high-temperature and strongly reducing environment), resulting in positive Eu anomalies (Bau, 1991). The bulk sediments and phases extracted in steps 1–5 exhibit no obvious positive Eu anomaly, indicating the sediments were not affected by hydrothermal activity (Table S1 and 1; Fig. 2).

##### 4.2.1. Carbonate

The carbonate phase has large negative Ce anomalies at site 30 (site 30 ( $\delta\text{Ce} = 0.04\text{--}0.07$ ) and site 64 (0.02–0.05) (Table 1; Fig. 2E–F), which are larger than those of seawater ( $\delta\text{Ce} = 0.18$  at a water depth of 5663 m in the western Pacific; Deng et al., 2017). The larger negative Ce anomaly of the carbonate may be related to organic degradation (Deng et al., 2022), which preferentially releases Ce relative to the other light REEs into pore waters.

##### 4.2.2. Amorphous Fe—Mn phase ( $\text{Fe}_{\text{ox1}}$ )

Previous studies have proposed that Ce<sup>4+</sup> is preferentially scavenged onto Fe—Mn (oxyhydr)oxides, which results in a positive Ce anomaly (Moffett, 1990; Takahashi et al., 2007; Tanaka et al., 2010). Ce<sup>3+</sup> can be adsorbed onto the surface of Fe-bearing minerals, and Mn-bearing minerals can adsorb and then oxidize Ce<sup>3+</sup> to Ce<sup>4+</sup> in ferromanganese nodules (Marcus et al., 2018). Positive Ce anomalies have been proposed to form in two different ways in Fe—Mn-bearing minerals in the deep ocean: (1) initial surface adsorption of Ce<sup>3+</sup> and subsequent oxidation of soluble Ce<sup>3+</sup> to Ce<sup>4+</sup> by vernadite ( $\delta\text{-MnO}_2$ ) and incorporation into Mn (oxyhydr)oxide phases (Koeppenkastrop and De Carlo, 1992; De Carlo et al., 1998; Ohta and Kawabe, 2000; Pattan et al., 2005), which can incorporate more Ce<sup>4+</sup> relative to the other light REEs in seawater; and (2) a depositional environment characterized by strong and stable bottom currents and a low deposition rate, which results in continuous and long-term contact with oxygenated and relatively rapidly rejuvenated bottom waters rather than oxidation by vernadite (Mangini et al., 1990; Jiang et al., 2010). The  $\delta\text{Ce}$  values of  $\text{Fe}_{\text{ox1}}$  exhibit a weak or positive correlation with Mn + Fe at sites 30 and 64, respectively (Fig. 3F), suggesting that this Fe—Mn phase can scavenge Ce from seawater. Negative Ce anomalies can form in Mn (oxyhydr)oxides due to the involvement of organic matter (e.g., polysaccharides, Deng et al., 2020; desferrioxamine B, Kraemer et al., 2017; humates, Davranche et al., 2005).  $\text{Fe}_{\text{ox1}}$  has negative Ce anomalies at sites 30 ( $\delta\text{Ce} = 0.40\text{--}0.47$ ) and 64 (0.24–0.77) (Table 1; Fig. 2E–F), possibly due to acetic acid-extracted residues (step 1) or factors unrelated to a reducing depositional environment. Given that  $\text{Fe}_{\text{ox1}}$  has a high content of amorphous Mn minerals, and that a large amount of  $\text{Fe}_{\text{ox1}}$  has transformed into  $\text{Fe}_{\text{ox2}}$  ( $\text{Fe}_{\text{Feox2}}/\text{Fe}_{\text{Feox1}} = 2.74\text{--}4.23$  at site 30 and 1.16–2.18 at site 64), the conditions were likely oxidizing and therefore the reduction of Fe—Mn (oxyhydr) oxide minerals did not occur. The  $\Sigma\text{REY}$  contents increase gradually as

$\delta\text{Ce}$  decreases (Fig. 3G).

#### 4.2.3. Crystalline iron phase (reducible iron; $\text{Fe}_{\text{ox2}}$ )

$\text{Fe}_{\text{ox2}}$  has variable Ce anomalies at sites 30 ( $\delta\text{Ce} = 0.61\text{--}1.04$ ) and 64 ( $\delta\text{Ce} = 0.24\text{--}2.30$ ) (Table 1; Fig. 2E–F). The  $\delta\text{Ce}$  values of  $\text{Fe}_{\text{ox2}}$  exhibit a positive correlation with the  $\delta\text{Ce}$  values of  $\text{Fe}_{\text{ox1}}$  (Fig. 3I), possibly due to the transformation of  $\text{Fe}_{\text{ox1}}$  to  $\text{Fe}_{\text{ox2}}$ , which releases more LREE<sup>3+</sup> relative to Ce.

## 5. Conclusions

In this study, we confirmed that clay-sized minerals in deep-sea sediments are a REY resource. Sequential chemical extraction of the clay-sized fraction of the sediments suggests that the REY are mainly hosted by amorphous Fe minerals and, to a lesser extent, by carbonate and crystalline Fe phases.

The carbonate may be authigenic and underwent early diagenetic organic degradation, and thus it inherited the REY characteristics of seawater by substitution for Ca<sup>2+</sup> and has larger negative Ce anomalies than seawater. The REY are probably bound to amorphous Fe (oxyhydr) oxides as free REY<sup>3+</sup> rather than Mn (oxyhydr)oxides. The  $\Sigma\text{REY}$  contents increase with more oxidizing conditions and the heavy REEs are more readily adsorbed to  $\text{Fe}_{\text{ox1}}$  under oxidizing conditions. The negative Ce anomalies of  $\text{Fe}_{\text{ox1}}$  may not be only due to the reduce conditions. Crystalline Fe may form by ageing of the amorphous Fe phase, and the light REEs are more readily released during this transformation. The heavy REEs are more readily retained on  $\text{Fe}_{\text{ox2}}$  under oxidizing conditions. The negative or positive Ce anomalies indicate that the transformation of  $\text{Fe}_{\text{ox1}}$  to  $\text{Fe}_{\text{ox2}}$  releases more REY<sup>3+</sup> than Ce.

## Software availability statement

Mineral composition and semi-quantitative calculations of clay-sized fractions were performed by MDI JADE 6 software.

## Credit author statement

Yan Liu: Writing - Review, Methodology, Project administration, Funding acquisition.

Yuntao Jing: Experiment; Writing - Original Draft & Editing.

Wancang Zhao: Methodology, Writing - Review.

## Declaration of Competing Interest

The authors declare that they have no known competing financial interests or personal relationships that could have appeared to influence the work reported in this paper.

## Data availability

The data in this research are available in Zenodo (doi: 10.5281/zenodo.7614706).

## Acknowledgements

This research was funded by the National Natural Science Foundation of China (Grants 92162216 and U2244222) and the China Geological Survey Program of the China Geological Survey, Ministry of Natural Resources (Grant DD 20221649).

## Appendix A. Supplementary data

Supplementary data to this article can be found online at <https://doi.org/10.1016/j.clay.2023.106876>.

## References

- Abbott, A.N., Löhr, S., Trethewy, M., 2019. Are clay minerals the primary control on the oceanic rare earth element budget? *Front. Mar. Sci.* 504, 19. <https://doi.org/10.3389/fmars.2019.00504>.
- Alibo, D.S., Nozaki, Y., 1999. Rare Earth elements in seawater: particle association, shale-normalization, and Ce oxidation. *Geochim. Cosmochim. Acta* 63, 363–372. [https://doi.org/10.1016/S0016-7037\(98\)00279-8](https://doi.org/10.1016/S0016-7037(98)00279-8).
- Anderson, L.A., Sarmiento, J.L., 1995. Global ocean phosphate and oxygen simulations. *Glob. Biogeochem. Cycles* 9, 621–636. <https://doi.org/10.1029/95GB01902>.
- Bau, M., 1991. Rare-earth element mobility during hydrothermal and metamorphic fluid-rock interaction and the significance of the oxidation state of europium. *Chem. Geol.* 93 (3–4), 219–230. [https://doi.org/10.1016/0009-2541\(91\)90115-8](https://doi.org/10.1016/0009-2541(91)90115-8).
- Bau, M., 1999. Scavenging of dissolved yttrium and rare earths by precipitating iron oxyhydroxide: experimental evidence for Ce oxidation, Y-Ho fractionation, and lanthanide tetrad effect. *Geochim. Cosmochim. Acta* 63 (1), 67–77. [https://doi.org/10.1016/S0016-7037\(99\)00014-9](https://doi.org/10.1016/S0016-7037(99)00014-9).
- Bi, D.J., Shi, X.F., Huang, M., Yu, M., Zhou, T.C., Zhang, Y., et al., 2021. Geochemical and mineralogical characteristics of deep-sea sediments from the western North Pacific Ocean: constraints on the enrichment processes of rare earth elements. *Ore Geol. Rev.* 138, 104318. <https://doi.org/10.1016/j.oregeorev.2021.104318>.
- Borer, P., Hug, S.J., Sulzberger, B., Kraemer, S.M., Kretzschmar, R., 2009. ATR-FTIR spectroscopic study of the adsorption of desferrioxamine B and aerobactin to the surface of lepidocrocite ( $\gamma$ -FeOOH). *Geochim. Cosmochim. Acta* 73, 4661–4672. <https://doi.org/10.1016/j.gca.2009.05.048>.
- Cao, C., Liu, X.M., Chen, J., 2022. Cerium anomaly as a tracer for paleoceanic redox conditions: a thermodynamics-based Ce oxidation modeling approach. *Front. Earth Sci.* 10, 927826. <https://doi.org/10.3389/feart.2022.927826>.
- Cook, H., Johnson, P., Matti, J., Zemmel, I., 1975. IV. Methods of Sample Preparation, and X-Ray Diffraction Data Analysis, X-Ray Mineralogy Laboratory, Deep Sea Drilling Project. University of California, Riverside (Initial reports of the deep sea drilling project 25).
- Davranche, M., Pourret, O., Gruau, G., Dia, A., Coz-Bouhnik, M.L., 2005. Adsorption of REE (III)-humic complexes onto MnO<sub>2</sub>: experimental evidence for cerium anomaly and lanthanide-tetrad effect suppression. *Geochim. Cosmochim. Acta* 69, 4825–4835. <https://doi.org/10.1016/j.gca.2005.06.005>.
- De Carlo, E.H., Wen, X.Y., Irving, M., 1998. The influence of redox reactions on the uptake of dissolved Ce by suspended Fe and Mn oxide particles. *Aquat. Geochem.* 3, 357–389. <https://doi.org/10.1023/A:100964626181>.
- Deng, Y.N., Ren, J.B., Guo, Q.J., Cao, J., Wang, H.F., Liu, C.H., 2017. Rare earth element geochemistry characteristics of seawater and porewater from deep sea in western Pacific. *CSci. Rep.* 7, 16539. <https://doi.org/10.1038/s41598-017-16379-1>.
- Deng, Y., Guo, Q., Liu, C., He, G., Cao, J., Liao, J., Liu, C., Wang, H., Zhou, J., Liu, Y., Wang, F., Zhao, B., Wei, R., Zhu, J., Qiu, H., 2022. Early diagenetic control on the enrichment and fractionation of rare earth elements in deep-sea sediments. *Sci. Adv.* 8, eabn5466. <https://doi.org/10.1126/sciadv.abn5466>.
- Deng, G., Ma, T., Tanaka, K., Ohnuki, T., Qiu, X., Yu, Q., 2020. Saccharide-mediated transformation of Ce during the formation of manganese (hydr)oxide. *Geochim. Cosmochim. Acta* 286, 143–158. <https://doi.org/10.1016/j.gca.2020.07.028>.
- Dymond, J., Ekland, W., 1978. A microprobe study of metalliferous sediment components. *Earth Planet. Sci. Lett.* 40 (2), 243–251. [https://doi.org/10.1016/0012-821X\(78\)90094-8](https://doi.org/10.1016/0012-821X(78)90094-8).
- Dzombak, D.A., Morel, F.M.M., 1990. Surface Complexation Modeling: Hydrous Ferric Oxide. Wiley, New York, pp. 81–95.
- Eggins, S.M., Woodhead, J.D., Kinsley, L.P.J., Mortimer, G.E., Sylvester, P., McCulloch, M.T., Hergt, J.M., Handler, M.R., 1997. A simple method for the precise determination of 40 trace elements in geological samples by ICPMS using enriched isotope internal standardisation. *Chem. Geol.* 134 (4), 311–326. [https://doi.org/10.1016/S0009-2541\(96\)00100-3](https://doi.org/10.1016/S0009-2541(96)00100-3).
- Gromet, L.P., Dyer, R.F., Haskin, L.A., Korotev, R.L., 1984. The “North American shale composition”: its complication, major and trace element characteristics. *Geochim. Cosmochim. Acta* 48, 2469–2482. [https://doi.org/10.1016/0016-7037\(84\)90298-9](https://doi.org/10.1016/0016-7037(84)90298-9).
- Guan, Y., Sun, X.M., Jiang, X.D., Sa, R., Zhou, L., Huang, Y., et al., 2017. The effect of Fe-Mn minerals and seawater interface and enrichment mechanism of ore-forming elements of polymetallic crusts and nodules from the South China Sea. *Acta Oceanol. Sin.* 36 (6), 34–46. <https://doi.org/10.1007/s13131-017-1004-4>.
- Halbach, P., Puteanus, D., 1984. The influence of the carbonate dissolution rate on the growth and composition of co-rich ferromanganese crusts from central pacific seamount areas. *Earth Planet. Sci. Lett.* 68 (1), 73–87. [https://doi.org/10.1016/0012-821X\(84\)90141-9](https://doi.org/10.1016/0012-821X(84)90141-9).
- Haley, B.A., Klinkhammer, G.P., McManus, J., 2004. Rare earth elements in pore waters of marine sediments. *Geochim. Cosmochim. Acta* 68, 1265–1279. <https://doi.org/10.1016/j.gca.2003.09.012>.
- Hathorne, E.C., Stichel, T., Brück, B., Frank, M., 2015. Rare earth element distribution in the Atlantic sector of the Southern Ocean: the balance between particle scavenging and vertical supply. *Mar. Chem.* 177, 157–171. <https://doi.org/10.1016/J.MARCHEM.2015.03.011>.
- Hein, J.R., Koschinsky, A., 2014. Deep-ocean ferromanganese crusts and nodules. In: Turekian, H.D.H.K. (Ed.), Treatise on Geochemistry, 2nd ed. Elsevier, Oxford, pp. 273–291.
- Hochella Jr., M.F., 1990. Atomic structure, microtopography, composition, and reactivity of mineral surfaces. In: Hochella Jr., M.F., White, A.F. (Eds.), Mineral-Water Interface Geochemistry: Reviews in Mineralogy, vol. 23. Mineralogical Society of America, Washington D C, pp. 87–132.
- Iijima, K., Yasukawa, K., Fujinaga, K., Nakamura, K., Machida, S., Takara, Y., et al., 2016. Discovery of extremely REY-rich mud in the western North Pacific Ocean. *Geochim. J.* 50, 557–573. <https://doi.org/10.2343/geochemj.2.0431>.
- Ji, J., Chen, J., Lu, H.Y., 1999. Origin of illite in the loess from the Luochuan area, Loess Plateau, Central China. *Clay Miner.* 34 (4), 525–532. <https://doi.org/10.1180/000985599546398>.
- Jiang, X.J., Lin, X.H., Yao, D., Guo, W.D., 2011. Enrichment mechanisms of rare earth elements in marine hydrogenic ferromanganese crusts. *Sci. China Earth Sci.* 54, 197–203. <https://doi.org/10.1007/s11430-010-4070-4>.
- Kamber, B.S., Greig, A., Schoenberg, R., Collerson, K.D., 2003. A refined solution to Earth's hidden niobium: Implications for evolution of continental crust and mode of core formation. *Precambr. Res.* 126, 289–308. [https://doi.org/10.1016/S0301-9268\(03\)00100-1](https://doi.org/10.1016/S0301-9268(03)00100-1).
- Kato, Y., Fujinaga, K., Nakamura, K., Takaya, Y., Kitamura, K., Ohta, J., et al., 2011. Deep-sea mud in the Pacific Ocean as a potential resource for rare-earth elements. *Nat. Geosci.* 4, 535–539. <https://doi.org/10.1038/ngeo1185>.
- Kim, M.G., Hyeong, K., Yoo, C.M., 2022. Distribution of rare earth elements and yttrium in sediments from the Clarion-Clipperton Fracture Zone, northeastern Pacific Ocean. *Geochim. Geophys. Geosyst.* 23 <https://doi.org/10.1029/2022GC010454>.
- Koeppenkastrop, D., De Carlo, E.H., 1992. Sorption of rare earth elements from seawater onto synthetic mineral particles: an experimental approach. *Chem. Geol.* 95, 251–263. [https://doi.org/10.1016/0009-2541\(92\)90015-W](https://doi.org/10.1016/0009-2541(92)90015-W).
- Kon, Y., Hoshino, M., Sanematsu, K., Morita, S., Tsunematsu, M., Okamoto, N., et al., 2014. Geochemical characteristics of apatite in heavy REE-rich deep-sea mud from Minami-Torishima Area, Southeastern Japan. *Resour. Geol.* 64, 47–57. <https://doi.org/10.1111/rge.12026>.
- Koschinsky, A., Halbach, P., 1995. Sequential leaching of marine ferromanganese precipitates: Genetic implications. *Geochim. Cosmochim. Acta* 59 (24), 5113–5132. [https://doi.org/10.1016/0016-7037\(95\)00358-4](https://doi.org/10.1016/0016-7037(95)00358-4).
- Koschinsky, A., Hein, J.R., 2003. Uptake of elements from seawater by ferromanganese crust: solid-phase associations and seawater speciation. *Mar. Geol.* 198, 331–351. [https://doi.org/10.1016/S0025-3227\(03\)00122-1](https://doi.org/10.1016/S0025-3227(03)00122-1).
- Kosmulski, M., 2011. The pH-dependent surface charging and points of zero charge: V. Update. *J. Colloid Interface Sci.* 353, 1–15. <https://doi.org/10.1016/j.jcis.2010.08.023>.
- Kraemer, D., Tepe, N., Pourret, O., Bau, M., 2017. Negative cerium anomalies in manganese (hydr)oxide precipitates due to cerium oxidation in the presence of dissolved siderophores. *Geochim. Cosmochim. Acta* 196, 197–208. <https://doi.org/10.1016/j.gca.2016.09.018>.
- Lawrence, M.G., Greig, A., Collerson, K.D., Kamber, B.S., 2006. Direct quantification of rare earth element concentrations in natural waters by ICP-MS. *Applied Geochem.* 21, 839–848. <https://doi.org/10.1016/j.apgeochem.2006.02.013>.
- Li, X., Sheng, A., Ding, Y., Liu, J., 2022. A model towards understanding stabilities and crystallization pathways of iron (oxyhydr)oxides in redox-dynamic environments. *Geochim. Cosmochim. Acta* 336, 92–103. <https://doi.org/10.1016/j.gca.2022.09.002>.
- Liao, J.L., Sun, X.M., Li, D.F., Sa, R.N., Lu, Y., Lin, Z.Y., et al., 2019a. New insights into nanostructure and geochemistry of bioapatite in REE-rich sediments: LA-ICP-MS, TEM, and Z-contrast imaging studies. *Chem. Geol.* 512, 58–68. <https://doi.org/10.1016/j.chemgeo.2019.02.039>.
- Liao, J.L., Sun, X.M., Wu, Z.W., Sa, R., Guan, Y., Lu, Y., et al., 2019b. Fe-Mn (oxyhydr) oxides as an indicator of REY enrichment in the deep-sea sediments from the central North Pacific. *Ore Geol. Rev.* 112, 103044. <https://doi.org/10.1016/j.oregeorev.2019.103044>.
- Liao, J.L., Chen, J.Y., Sun, X.M., Wu, Z.W., Deng, Y.N., Shi, X.F., et al., 2022. Quantifying the controlling mineral phases of rare-earth elements in deep-sea pelagic sediments. *Chem. Geol.* 595, 120792. <https://doi.org/10.1016/j.chemgeo.2022.120792>.
- Lu, W.Y., Zhao, W.C., Balsam, W., Lu, H.Y., Liu, P., Lu, Z.L., Ji, J.F., 2017. Iron mineralogy and speciation in clay-sized fractions of Chinese desert sediments. *J. Geophys. Res.-Atmos.* 122, 13,458–13,471. <https://doi.org/10.1002/2017JD027733>.
- Mangini, A., Segl, M., Glasby, G.P., Stoffers, P., Plüger, W.L., 1990. Element accumulation rates and growth histories of manganese nodules from the Southwestern Pacific Basin. *Mar. Geol.* 94, 97–107. [https://doi.org/10.1016/0025-3227\(90\)90105-S](https://doi.org/10.1016/0025-3227(90)90105-S).
- Marcus, M.A., Toner, B.M., Takahashi, Y., 2018. Forms and distribution of Ce in a ferromanganese nodule. *Mar. Chem.* 202 (20), 58–66. <https://doi.org/10.1016/j.marchem.2018.03.005>.
- Mehra, O., Jackson, M., 1958. Iron oxide removal from soils and clays by a dithiomcitrate system buffered with sodium bicarbonate. *Natl. Conf. Clays Clays Miner.* 7 (1), 317–327. <https://doi.org/10.1016/B978-0-08-009235-5.50026-7>.
- Moffett, J.W., 1990. Microbially mediated cerium oxidation in sea water. *Nature* 345 (6274), 421–423. <https://doi.org/10.1038/345421a0>.
- Moore, D.M., Reynolds, R.C., 1997. X-Ray Diffraction and the Identification and Analysis of Clay Minerals, 2nd ed. Oxford University Press, Oxford.
- Ohta, A., Kawabe, I., 2000. REE (III) adsorption onto Mn dioxide ( $\delta$ -MnO<sub>2</sub>) and Fe oxyhydroxide: Ce (III) oxidation by  $\delta$ -MnO<sub>2</sub>. *Geochim. Cosmochim. Acta* 65, 695–703. [https://doi.org/10.1016/S0016-7037\(00\)00578-0](https://doi.org/10.1016/S0016-7037(00)00578-0).
- Ohta, J., Yasukawa, K., Machida, S., Fujinaga, K., Nakamura, K., Takaya, Y., et al., 2016. Geological factors responsible for REY-rich mud in the western North Pacific Ocean: implications from mineralogy and grain size distributions. *Geochem. J.* 50, 591–603. <https://doi.org/10.2343/geochemj.2.0435>.
- Pattan, J.N., Pearce, N.J.G., Mislankar, P.G., 2005. Constraints in using Cerium-anomaly of bulk sediments as an indicator of paleo bottom water redox environment: a case

- study from the Central Indian Ocean Basin. *Chem. Geol.* 221 (3–4), 260–278. <https://doi.org/10.1016/j.chemgeo.2005.06.009>.
- Poulton, S.W., Canfield, D.E., 2005. Development of a sequential extraction procedure for iron: implications for iron partitioning in continental derived particulates. *Chem. Geol.* 214, 209–221. <https://doi.org/10.1016/j.chemgeo.2004.09.003>.
- Raiswell, R., Canfield, D.E., 2012. The iron biogeochemical cycle past and present. *Geochem. Perspect.* 1, 1–220. <https://doi.org/10.7185/geochempersp.1.1>.
- Ren, J.B., Liu, Y., Wang, F.L., He, G.W., Deng, X.G., Wei, Z.Q., Yao, H.Q., 2021. Mechanism and influencing factors of REY enrichment in deep-sea sediments. *Minerals* 11, 196. <https://doi.org/10.3390/min11020196>.
- Ren, J.B., Jiang, X.X., He, G.W., Wang, F.L., Yang, T.B., Luo, S.J., et al., 2022. Enrichment and sources of REY in phosphate fractions: constraints from the leaching of REY-rich deep-sea sediments. *Geochim. Cosmochim. Acta* 335, 155–168. <https://doi.org/10.1016/j.gca.2022.08.035>.
- Rong, K., Zeng, Z., Yin, X., Chen, S., Wang, X., Qi, H., Ma, Y., 2018. Smectite formation in metalliferous sediments near the East Pacific Rise at 13°N. *Acta Oceanol. Sin.* 37 (9), 67–81. <https://doi.org/10.1007/s13131-018-1265-6>.
- Ruttenberg, K.C., 1992. Development of a sequential extraction method for different forms of phosphorus in marine sediments. *Limnol. Oceanogr.* 37, 1460–1482. <https://doi.org/10.4319/lo.1992.37.7.1460>.
- Sa, R., Sun, X.M., He, G.W., Xu, L., Pan, Q.Q., Liao, J.L., Zhu, K.C., Deng, X.G., 2018. Enrichment of rare earth elements in siliceous sediments under slow deposition: a case study of the central North Pacific. *Ore Geol. Rev.* 94, 12–23. <https://doi.org/10.1016/j.oregeorev.2018.01.019>.
- Schindler, P.W., Stumm, W., 1987. The surface chemistry of oxides, hydroxides, and oxides minerals. In: Stumm, W. (Ed.), *Aquatic Surface Chemistry. Chemical processes at the Particle-Water Interface*. John Wiley and Sons, New York, pp. 83–110.
- Sheng, A., Liu, J., Li, X.X., Qafoku, O., Collins, R.N., Jones, A.M., et al., 2020. Labile Fe (III) from sorbed Fe(II) oxidation is the key intermediate in Fe(II)-catalyzed ferrihydrite transformation. *Geochim. Cosmochim. Acta* 272, 105–120. <https://doi.org/10.1016/j.gca.2019.12.028>.
- Shi, N.C., Ma, Z.S., He, W.Z., Luo, J.M., 1995. Nano-solids in manganese nodules from northern part of Pacific Ocean floorNano-solids in minerals and prospects of its uses in industry. *Sci. China Ser. B Chem.* 38 (12), 1493–1500.
- Shi, X.F., Bi, D.J., Huang, M., Yu, M., Luo, Y.M., Zhou, T.C., Zhang, Z.Q., Liu, J.H., 2021. Distribution and metallogenesis of deep-sea rare earth element. *Geol. Bull. China* 40, 195–208 (in Chinese with English abstract).
- Stumm, W., 1992. Chemistry of the Solid-Water Interface: Processes at the Mineral-Water and Particle-Water Interface in Natural Systems. John Wiley and Sons, New York.
- Takahashi, Y., Manceau, A., Geoffroy, N., Marcus, M.A., Usui, A., 2007. Chemical and structural control of the partitioning of Co, Ce, and Pb in marine ferromanganese oxides. *Geochim. Cosmochim. Acta* 71, 984–1008. <https://doi.org/10.1016/j.gca.2006.11.016>.
- Stumm, W., Sulzberger, B., 1992. The cycling of iron in natural environments: Considerations based on laboratory studies of heterogeneous redox processes. *Geochim. Cosmochim. Acta* 56 (8), 3233–3257. [https://doi.org/10.1016/0016-7037\(92\)90301-X](https://doi.org/10.1016/0016-7037(92)90301-X).
- Takaya, Y., Fujinaga, K., Yamagata, N., Araki, S., Maki, R., Nakamura, K., Iijima, K., Kato, Y., 2015. Chemical leaching of rare earth elements from highly REY-rich mud. *Geochem. J.* 49, 637–652. <https://doi.org/10.2343/geochemj.2.0373>.
- Takaya, Y., Yasukawa, K., Kawasaki, T., Fujinaga, K., Ohta, J., Usui, Y., et al., 2018. The tremendous potential of deep-sea mud as a source of rare-earth elements. *Sci. Rep.* 8 (1), 5763. <https://doi.org/10.1038/s41598-018-23948-5>.
- Tamura, H., Mita, K., Tanaka, A., Ito, M., 2001. Mechanism of hydroxylation of metal oxide surfaces. *J. Colloid Interface Sci.* 243 (1), 202–207. <https://doi.org/10.1006/jcis.2001.7864>.
- Tanaka, K., Tani, Y., Takahashi, Y., Tanimizu, M., Suzuki, Y., Kozai, N., Ohnuki, T., 2010. A specific Ce oxidation process during sorption of rare earth elements on biogenic Mn oxide produced by *Acronymium* sp. strain KR21-2. *Geochim. Cosmochim. Acta* 74, 5463–5477. <https://doi.org/10.1016/j.gca.2010.07.010>.
- Tanaka, E., Nakamura, K., Yasukawa, K., Mimura, K., Fujinaga, K., Ohta, J., et al., 2020. Chemostratigraphic correlations of deep-sea sediments in the western North Pacific Ocean: a new constraint on the distribution of mud highly enriched in rare-earth elements. *Minerals* 10 (6), 575. <https://doi.org/10.3390/min10060575>.
- Tang, J.W., Johannesson, K.H., 2005. Adsorption of rare earth elements onto Carrizo sand: experimental investigations and modeling with surface complexation. *Geochim. Cosmochim. Acta* 69, 5247–5261. <https://doi.org/10.1016/j.gca.2005.06.021>.
- Voigt, M., Mavromatis, V., Oelkers, E.H., 2017. The experimental determination of REE partition coefficients in the water-calcite system. *Chem. Geol.* 462, 30–43. <https://doi.org/10.1016/j.chemgeo.2017.04.024>.
- Yasukawa, K., Liu, H., Fujinaga, K., Machida, S., Haraguchi, S., Ishii, T., Nakamura, K., Kato, Y., 2014a. Geochemistry and mineralogy of REY-rich mud in the eastern Indian Ocean. *J. Asian Earth Sci.* 93, 25–36. <https://doi.org/10.1016/j.jseas.2014.07.005>.
- Yasukawa, K., Liu, H., Fujinaga, K., Machida, S., Haraguchi, S., Ishii, T., et al., 2014b. Geochemistry and mineralogy of REY-rich mud in the eastern Indian Ocean. *J. Asian Earth Sci.* 93, 25–36. <https://doi.org/10.1016/j.jseas.2014.07.005>.
- Yasukawa, K., Kino, S., Azami, K., Tanaka, E., Mimura, K., Ohta, J., et al., 2020. Geochemical features of Fe-Mn micronodules in deep-sea sediments of the western North Pacific Ocean: potential for co-product metal extraction from REY-rich mud. *Ore Geol. Rev.* 127, 103805. <https://doi.org/10.1016/j.oregeorev.2020.103805>.
- Zawadzki, D., Maciąg, Ł., Abramowski, T., McCartney, K., 2020. Fractionation trends and variability of rare earth elements and selected critical metals in pelagic sediment from abyssal basin of NE Pacific (Clarion-Clipperton Fracture Zone). *Minerals* 10 (4), 320. <https://doi.org/10.3390/min10040320>.
- Zhang, K., Shields, G.A., 2022. Sedimentary Ce anomalies: secular change and implications for paleoenvironmental evolution. *Earth-Sci. Rev.* 229, 104015. <https://doi.org/10.1016/j.earscirev.2022.104015>.
- Zhao, Y., Zou, X., Gao, J., Wang, C., Li, Y., Yao, Y., Zhao, W., Xu, M., 2018. Clay mineralogy and source-to-sink transport processes of Changjiang river sediments in the estuarine and inner shelf areas of the East China Sea. *J. Asian Earth Sci.* 152, 91–102. <https://doi.org/10.1016/j.jseas.2017.11.038>.
- Zhou, T.C., Shi, X.F., Huang, M., Yu, M., Bi, D.J., Ren, X.W., Yang, G., Zhu, A.M., 2020. The influence of hydrothermal fluids on the REY-rich deep-sea sediments in the Yungan Basin, Eastern South Pacific Ocean: constraints from bulk sediment geochemistry and mineralogical characteristics. *Minerals* 10, 1141. <https://doi.org/10.3390/min10121141>.
- Zhou, T.C., Shi, X.F., Huang, M., Yu, M., Bi, D.J., Ren, X.W., et al., 2021. Genesis of REY-rich deep-sea sediments in the Tiki Basin, eastern South Pacific Ocean: evidence from geochemistry, mineralogy and isotope systematics. *Ore Geol. Rev.* 138, 104330. <https://doi.org/10.1016/j.oregeorev.2021.104330>.